

Article

Discrete-Time Fractional Order Integral Sliding Mode Control of an Antagonistic Actuator Driven by Pneumatic Artificial Muscles

Quy-Thinh Dao ^{1,2,*} , Manh-Linh Nguyen ²  and Shin-ichiroh Yamamoto ³¹ Graduate School of Engineering and Science, Shibaura Institute of Technology, Saitama 337-8570, Japan² Department of Industrial Automation, Hanoi University of Science and Technology, Ha Noi 11615, Vietnam; linh.nguyenmanh@hust.edu.vn³ Department of Bioscience and Engineering, Shibaura Institute of Technology, Saitama 337-8570, Japan; yamashin@se.shibaura-it.ac.jp

* Correspondence: nb16505@shibaura-it.ac.jp or think.daoquy@hust.edu.vn; Tel.: +81-80-9307-9301

Received: 22 May 2019; Accepted: 18 June 2019; Published: 19 June 2019



Abstract: Recently, pneumatic artificial muscles (PAMs), a lightweight and high-compliant actuator, have been increasingly used in assistive rehabilitation robots. PAM-based applications must overcome two inherent drawbacks. The first is the nonlinearity due to the compressibility of the air, and the second is the hysteresis due to its geometric construction. Because of these drawbacks, it is difficult to construct not only an accurate mathematical model but also a high-performance control scheme. In this paper, the discrete-time fractional order integral sliding mode control approach is investigated to deal with the drawbacks of PAMs. First, a discrete-time second order plus dead time mathematical model is chosen to approximate the characteristics of PAMs in the antagonistic configuration. Then, the fractional order integral sliding mode control approach is employed together with a disturbance observer to improve the trajectory tracking performance. The effectiveness of the proposed control method is verified in multi-scenario experiments using a physical actuator.

Keywords: pneumatic artificial muscle; sliding mode control; fractional calculus; antagonistic actuator

1. Introduction

In recent years, high-compliant and low-cost pneumatic artificial muscles (PAMs) have been widely implemented in rehabilitation systems [1–4]. PAMs are shortened in the longitudinal direction and enlarged in the radial direction when being inflated, and they will turn back to their initial form when being completely deflated. PAMs act similar to the human muscle, e.g., the longer muscles produce bigger force and vice versa. Furthermore, these pneumatic muscles are also inherently compliant, which makes them suitable for applying in human-robotic systems. In comparison with the motorized actuators, PAMs are lightweight and have a high power-to-weight ratio. In addition to the aforementioned advantages, the PAM-based applications also have inherent drawbacks, such as very high nonlinearity and uncertainty, and slow response in force generation. These drawbacks make it difficult to model and control PAMs.

Using a nonlinear mathematical model to describe the nonlinear characteristic of the PAMs is the most common choice of researchers. In 2003, D. B. Reynolds et al. introduced a three-elements model of PAM, which consists of a contractile (force-generating) element, spring element, and damping element in parallel [5]. Using this type of model, K. Xing et al. developed the sliding mode control (SMC) based on a nonlinear disturbance observer to improve the tracking performance of a single PAM-mass system [6]. A boundary layer augmented SMC and its modified versions have also been developed for both antagonistic configuration of PAMs and robot orthosis actuated by PAMs [4,7–12].

However, the procedure to identify this model's parameters remains complicated with at least two separate experiments: one experiment for determining spring (K) and contractile (F) coefficients and another experiment for estimating damping (B) coefficient. Each experiment must be carried out in three steps [6]. Besides, the parameters of the damping (B) coefficient must be obtained by measuring the load's acceleration, which is very sensitive to external noise. For this reason, it is difficult to obtain the model's parameters with high accuracy.

To deal with hysteresis of PAMs, many hysteresis models have been proposed recently, e.g., Maxwell-slip model [13], Prandtl–Ishlinskii model [14], and Preisach model [15]. In these reports, the dynamic characteristic of PAMs was described by an equivalent pressure/length hysteresis model. The obtained models were used in the feedforward term of the cascade position control scheme for hysteresis compensation. The inner loop of the controllers was designed to regulate the inside pressure of the muscles. The outer loops were designed to deal with the nonlinearity of the PAMs characteristic. Both of the loops use PID-based control strategy. Consequently, some authors continued to develop the modified hysteresis model for both single PAM-mass system and PAMs in antagonistic configuration [16,17]. However, they mainly focused on modelling of PAMs. Only the trajectory-tracking experiments with low frequency, e.g., up to 0.2 Hz, were conducted in literature. Furthermore, enhanced PID control methods, which were most widely used in these studies, could not deal with hysteresis of PAMs.

Another common way to identify the model of PAM-based actuator is the grey-box experiment method [18–21]. In 2015, to deal with uncertain nonlinearity of PAMs, Dang Xuan Ba et al. introduced a grey-box experimental model, which consisted of uncertain, unknown, and nonlinear terms. Based on the built-in model, the authors employed a sliding mode control strategy [18] and an integrated intelligent nonlinear control approach [19] for the tracking purpose. The control performance was significantly improved, and the system could track the 10° amplitude sinusoidal signal with 1.5 Hz frequency. The grey-box method was also reported by Robinson et al. in 2016 [20] and by L. Cveticanin et al. in 2018 [21]. The relationships angle/torque and force/pressure were thoroughly investigated in the wide range of pressure. However, only the mathematical model was considered and verified in [20]. The low rate of desired trajectories was tracked in [21].

The mechanism-based model [22,23] is another method in which the behaviour of PAMs was described based on their physical properties: length, diameter, and volume of PAMs, etc. However, as most of nonlinear models mentioned above, these types of models also require a complex procedure to derive the model parameters.

To obtain the model of PAMs in a more simple way with a good enough accuracy, the linear mathematical model has recently been applied to approximate the characteristic of PAMs [24–28]. In these studies, the uncertain nonlinearity of PAM was considered as the system disturbance and solved by extended state observer (ESO) together with an active disturbance rejection controller (ADRC). The control performance is considerably improved with 0.5 Hz of sinusoidal reference signal frequency.

In this research, a discrete-time fractional order integral sliding mode control (DFISMC) is employed to improve tracking performance of an antagonistic actuator driven by PAMs. First, a linear discrete-time second order plus dead time (SOPDT) model is chosen to describe the nonlinear dynamic behaviour of the antagonistic actuator. In this approximation, a nonlinear term in characteristics of PAM is considered as a disturbance. Then, the DFISMC is designed based on the fractional order integral (FOI) calculus and a disturbance observer (DSO) for the trajectory tracking purpose. Finally, the effectiveness of the proposed control technique is confirmed through multi-scenario experiments. The proposed method shows many advantages in both mathematical model and control technique. The linear discrete-time SOPDT can approximate the behaviour of antagonistic actuator at a good accuracy. Besides, the identification procedure is also simplified. By employing the FOI function together with a DSO, the DFISMC controller is able to reduce the “chattering” problem in sliding mode

control systems. In addition, the proposed is designed in a discrete-time domain, therefore, it can be easily implemented by any digital control system.

2. System Description

2.1. Experiment Platform

A typical configuration of antagonistic configuration of PAMs is shown in Figure 1a, and the proposed experiment platform is demonstrated in Figure 1b. The experimental system consisted of two PAMs which had 1.0 inches of diameter and 22 inches of length. The PAMs were fabricated at our local institute. The pressure inside each PAMs was regulated by two proportional electric control valves series ITV 2030-212S-X26 from SMC company. One potentiometer CP-20H from Midori Precision (Japan) was used to measure the actuator’s angle. All the control systems were implemented by using computer-based controller NI cDAQ-9178 from National Instrument (USA). The real-time controller collected the data from the potentiometer via analogue input module and sends the control signal to the electric control valve via analogue output modules. The developed control algorithm was implemented and compiled by LabView software before downloading it to the hardware controller.

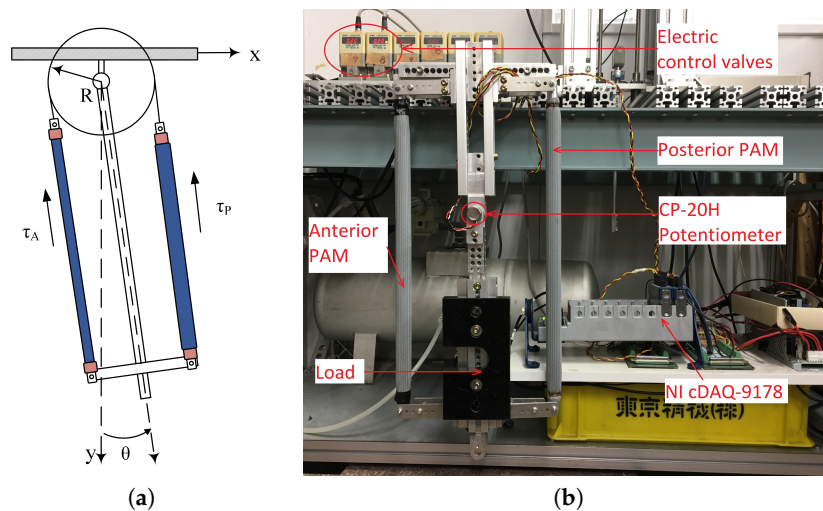


Figure 1. (a) Typical antagonistic configuration of two pneumatic artificial muscles (PAMs) and (b) experiment platform of an antagonistic actuator powered by PAMs.

2.2. System Modeling

Based on the geometry of the typical antagonistic configuration, which is illustrated in Figure 1a, the length of each PAMs can be obtained from the measured joint angle, as in the following equations:

$$y_A = y_{AN} + R\theta \tag{1a}$$

$$y_P = y_{PN} - R\theta, \tag{1b}$$

where y_{AN} and y_{PN} are the nominal length of the anterior and posterior PAMs when the joint angle $\theta = 0$, and R is the rotation radius of the actuator. Because two similar PAMs are used in the system, we can consider that $y_{AN} = y_{PN} = y_N$. Following that, the relationship between contraction of PAMs and the measured angle can be expressed as

$$\epsilon_A = \frac{y_0 - y_A}{y_0} \times 100\% = \frac{y_0 - (y_N + R\theta)}{y_0} \times 100\% \tag{2a}$$

$$\epsilon_P = \frac{y_0 - y_P}{y_0} \times 100\% = \frac{y_0 - (y_N - R\theta)}{y_0} \times 100\% \tag{2b}$$

where y_0 is the length of PAMs in the complete deflation state. In (2), y_0 and y_N are fixed by the deflation and nominal lengths of PAMs. Therefore, the contraction of PAMs can be expressed as the function of the measured joint angle θ . As a result, the dynamic behaviour of an antagonistic muscle can be described by a single input single output (SISO) system, in which the input is the difference pressure of two PAMs (ΔP), and the output is the measured angle θ . The input pressure inside the anterior and posterior PAMs can be expressed as

$$P_P = P_0 + \Delta P \tag{3a}$$

$$P_A = P_0 - \Delta P, \tag{3b}$$

where P_0 is the nominal pressure which determines the initial position of antagonistic actuator. The nominal pressure can be chosen so that the joint has the desired compliance for a specific application. It was fixed, so ΔP was chosen as a control variable of trajectory-tracking controller. All the system parameters P_0 , y_0 , and y_N are provided as in Table 1. In this research, the following discrete-time SISO system was chosen to describe the model of antagonistic actuator:

$$y_{k+1} = - \sum_{i=1}^n a_i y_{k-i+1} + \sum_{j=1}^m b_j u_{k-j-d+1} + p_k, \tag{4}$$

where u_k represents the control pressure ΔP , y_k is the joint angle, d is a positive integer representing the dead time of the system (as a number of the sampling time), p_k is the unknown disturbance of the system, a_i and b_j are the model parameters with $b_1 \neq 0$, n and m are integers which satisfy $n \leq m$. The model parameters of the system are obtained by the identification experiment. To verify the mathematical model of PAM, the following experiment procedure was carried out.

Step 1: The initial position of the actuator was set at 0° by supplying nominal pressure P_0 to each PAMs of the actuator.

Step 2: The actuator angle can be changed by sending different types of control signal to the electrical control valves. Three types of control signals were used in this experiment:

- Step response: the control signal was a step wave with the final values 0.2, 0.4, 0.5, and 0.8 MPa.
- Sinusoidal signal: The control signal is the 0.2 MPa amplitude sinusoidal signal, where frequency varies from 0.2 to 1.0 Hz.
- A sine wave signal with time-varying amplitude and frequency, as in the following equation:

$$u(t) = A \sin(2\pi f t) + 0.8 A \sin(2\pi 0.2 f t) + 0.5 A \sin(2\pi 1.5 f t) + 0.2 A \sin(2\pi 3 f t), \tag{5}$$

where $A = 0.05$ MPa and $f = 0.5$ Hz are the basis amplitude and frequency of the control signal, respectively.

All the data, including control signals and measured angles of actuator, were recorded with sampling time $T_s = 5$ ms for further analysis.

Step 3: The discrete-time SOPDT, in which $m = n = 2$, was chosen as the mathematical model of the actuator with good accuracy. The precise values of the model's parameters are estimated by using the MATLAB software and provided in Table 2.

Table 1. Initial parameters of pneumatic artificial muscles (PAMs).

Parameters	y_0 [in]	y_N [in]	P_0 [MPa]
Values	22	15	0.2

Table 2. Identified parameters of the antagonistic actuator.

Model Parameters	a_1	a_2	b_1	b_2	d
Value (Mean \pm SD)	-1.9139 ± 0.0182	0.9164 ± 0.0180	0.0472 ± 0.0064	0.0460 ± 0.0061	22 ± 3

Figure 2 shows identification results: (a) the control inputs are step of 0.4 MPa, (b) 0.5 Hz sine wave signal, and (c) time-varying amplitude and frequency sinusoidal signal. The discrete-time SOPDT mathematical model depicts a good approximation of nonlinear behaviour of the antagonistic actuator. The maximum error of the estimated angle (dash red line) from the measured one (blue line) was less than 5.0° , and the root mean square error did not exceed 2.5° . The mean values and standard deviations (SD) of the model parameters obtained by different types of control signals are provided in Table 2. As seen in Table 2, the standard deviations of the model parameters were much smaller than their mean values. Therefore, we can conclude that the model parameters obtained by different methods have similar values. As a result, we can use any aforementioned method for the identification purpose. The model parameters, which were identified by time-varying amplitude and frequency, are chosen to design the controller in Section 3 of this paper.

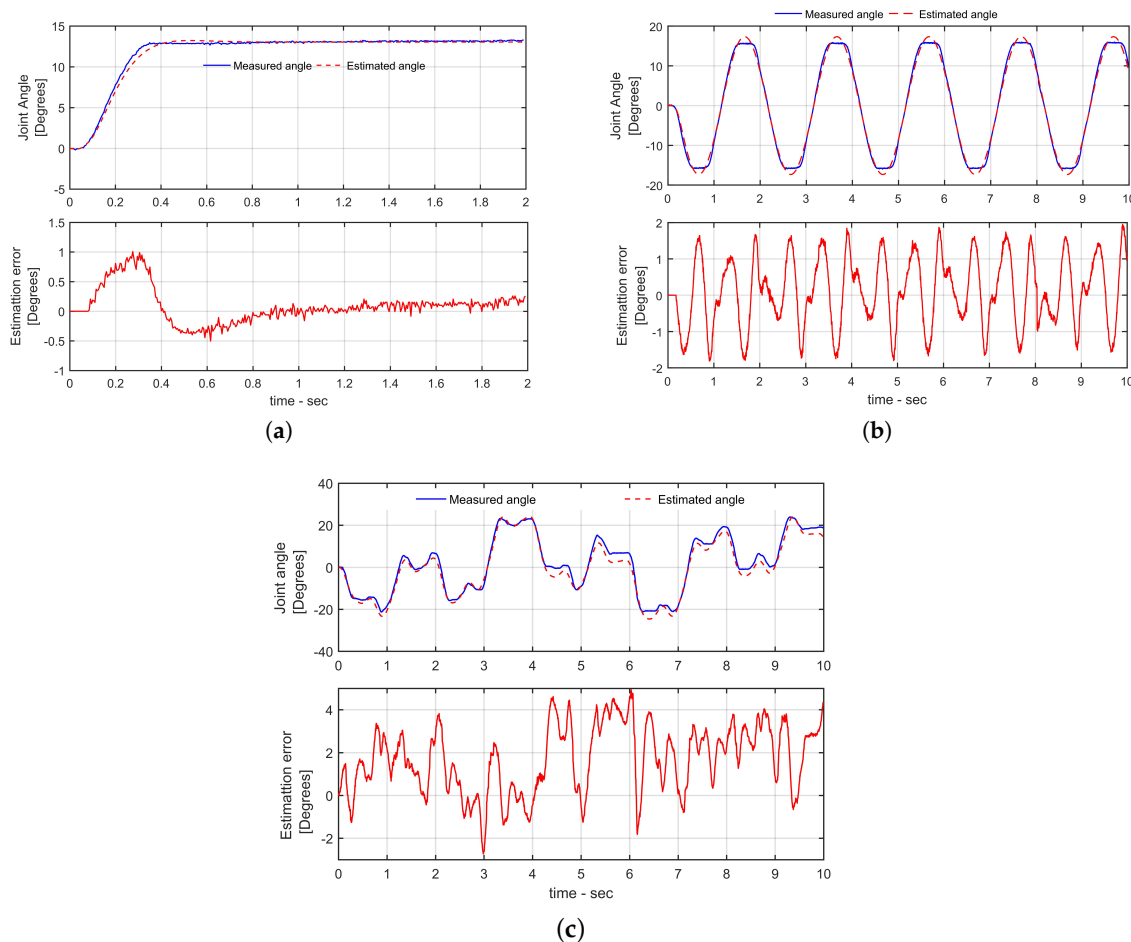


Figure 2. Identification results of the antagonistic actuator: (a) the step input of 0.4 MPa, (b) the 0.5 Hz sinusoidal signal, and (c) the time-varying amplitude and frequency control input. Upper sub-figures show measured (blue line) and estimated (dash red line) show value of the actuator angle. Lower sub-figures show the estimation error of the mathematical model.

3. Control Design

Recently, SMC has been employed for designing the controller for PAMs or systems powered by PAMs [4,6–11]. SMC is able to provide highly accurate tracking performance with a bounded error; however, “chattering” problem is a big challenge that SMC must overcome. SMC is a suitable control approach for PAM-based systems to deal with their uncertain, nonlinear and time varying characteristics. In this research, we addressed a DFISMC to improve the tracking performance of the antagonistic actuator powered by PAMs. The fractional order integral is implemented together with disturbance observer to deal with the “chattering” problem. Figure 3 illustrates the block diagram of the proposed control system.

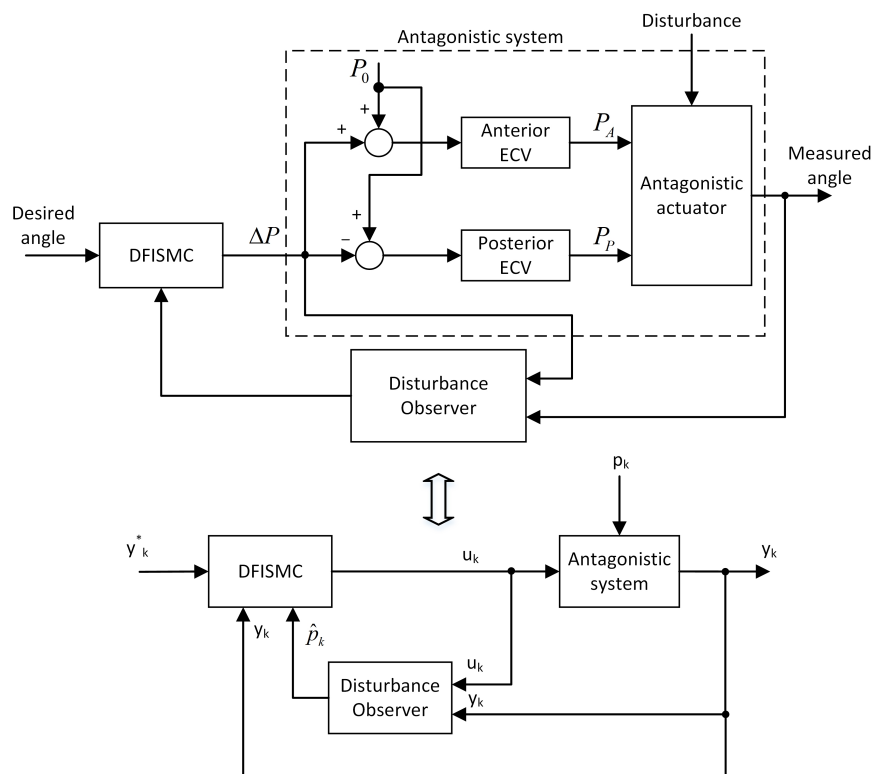


Figure 3. Block diagram of the discrete-time fractional integral sliding mode control.

We consider the following fractional integral sliding surface:

$$S_k = e_k + {}^\alpha \Xi_{e,k} \tag{6}$$

where $e_k = y_k^* - y_k$ is the tracking error with the desired trajectory y_k^* , and ${}^\alpha \Xi_{e,k}$ is the integral of the tracking error with fractional order α and integral gain K_I . ${}^\alpha \Xi_{e,k}$ can be calculated as follows:

$${}^\alpha \Xi_{e,k} = {}^\alpha \Xi_{e,k-1} + K_I \left(\sum_{j=2}^N \Omega_j \tilde{e}_{k-N+j} + \Omega_1 e_{k-N+1} \right) \tag{7}$$

and ${}^\alpha \Xi_{e,0} = \omega_N e_0$ at the initial state. Please refer to Appendix A for details about fractional integral approximation. We also obtain

$${}^\alpha \Xi_{e,k+1} = {}^\alpha \Xi_{e,k} + K_I \left(\sum_{j=2}^N \Omega_j \tilde{e}_{k-N+j+1} + \Omega_1 \tilde{e}_{k-N+2} \right) \tag{8}$$

From (6)–(8), we can obtain

$$S_{k+1} = e_{k+1} + S_k - e_k + K_I \left(\sum_{j=2}^N \Omega_j \tilde{e}_{k-N+j+1} + \Omega_1 \tilde{e}_{k-N+2} \right) \tag{9}$$

Therefore,

$$S_{k+1} - S_k = (1 + K_I \Omega_N) e_{k+1} - (1 + K_I \tilde{\Omega}_N) e_k - K_I \sum_{j=2}^{N-1} \tilde{\Omega}_j e_{k-N+j} \tag{10}$$

where $e_k + 1$ is one-step-ahead tracking error, which can be computed from the SISO model of the actuator in (4) as

$$e_{k+1} = y_{k+1}^* + \sum_{i=1}^n a_i y_{k-i+1} - \sum_{j=1}^m b_j u_{k-d-j+1} - p_k, \tag{11}$$

where y_{k+1}^* is one step ahead of the desired trajectory, which is considered to be known when apply the model to a specific application. In (4), disturbance p_k is unknown and needs to be estimated. In this study, one-step delayed technique was used to estimate p_k . This technique is based on the following assumptions:

Assumption 1. Sampling time T_s was sufficiently small and system disturbance p_k is bounded, so the difference between two consecutive time samples is also bounded, i.e.,

$$p_k - p_{k-1} = O(T_s) \tag{12}$$

$$p_k - 2p_{k-1} + p_{k-2} = O(T_s^2), \tag{13}$$

where $O(T_s)$ is the thickness boundary layer. It means there always exist constants A and B , $\forall k > 0$, such that

$$|p_k - p_{k-1}| \leq AT_s \tag{14}$$

$$|p_k - 2p_{k-1} + p_{k-2}| \leq BT_s^2. \tag{15}$$

The aforementioned assumption was based on the Taylor expansion described in Appendix B.

Estimation \hat{p}_k of disturbance p_k can be computed based on (4) as

$$\hat{p}_k = 2p_{k-1} - p_{k-2}, \tag{16}$$

where

$$p_{k-1} = y_k + \sum_{i=1}^n a_i y_{k-i} - \sum_{j=1}^m b_j u_{k-j}. \tag{17}$$

Hence, the error of estimation \tilde{p}_k is

$$\begin{aligned} \tilde{p}_k &= p_k - \hat{p}_k \\ &= p_k - 2p_{k-1} + p_{k-2} = O(T_s^2). \end{aligned} \tag{18}$$

Finally, the one-step-ahead tracking error (11) can be expressed by

$$e_{k+1} = y_{d,k+1} + \sum_{i=1}^n a_i y_{k-i+1} - \sum_{j=1}^m b_j u_{k-j+1} - \hat{p}_k - \tilde{p}_k. \tag{19}$$

When substituting e_{k+1} in (11) and $p_k = \hat{p}_k + \tilde{p}_k$ into (10), we can obtain

$$S_{k+1} - S_k = -(1 + K_I \tilde{\Omega}_N) e_k - K_I \sum_{j=2}^{N-1} \tilde{\Omega}_j e_{k-N+j} + (1 + K_I \Omega_N) \left(y_{k+1}^* + \sum_{i=1}^n a_i y_{k-i+1} - \sum_{j=1}^m b_j u_{k-j-d+1} - \hat{p}_k - \tilde{p}_k \right) \quad (20)$$

Disturbance estimation error \tilde{p}_k is unknown in practice; however, it is very small and bounded by assumption 1. Control signal u_k can be obtained by solving the reaching law $S_{k+1} = 0$ with the absence of \tilde{p}_k as follows:

$$u_k = b_1^{-1} \left(y_{k+1}^* + \sum_{i=1}^n a_i y_{k-i+1} - \sum_{j=1}^m b_j u_{k-j-d+1} - \hat{p}_k \right) - \frac{(1 + K_I \tilde{\Omega}_N) e_k - K_I \sum_{j=2}^{N-1} \tilde{\Omega}_j e_{k-N+j}}{b_1 (1 + K_I \Omega_N)}. \quad (21)$$

Adjusting integral gain K_I and fractional order integral α may improve performance of the control system.

4. Experimental Evaluation

4.1. Experimental Procedure

To verify the effectiveness of the proposed control method, multiple-scenario experiment with different desired trajectories was carried out. In the first scenario of the trajectory-tracking experiment, sinusoidal signals with amplitude 20° and 0.2, 0.5, 0.8, and 1 Hz frequency were given as desired trajectories. To evaluate the applicability of the proposed control method for a rehabilitation robot, a human-like pattern signal was employed as a desired trajectory in the second scenario of the experiment. The modified knee gait data profile in textbook [29], where the maximum flexion angle is set at 28° , was used to verify the control performance. In both experimental scenarios, the system was tested under two load conditions: no load and load $m = 2.5$ kg.

In all experimental scenarios, the sampling time of the discrete-time control system was $T_s = 5$ ms. All the data were recorded for ten cycles from the start time of the experiment. The data were processed by MATLAB software version R2016b. The proposed controller is also compared with the conventional discrete-time sliding mode control (DSMC) method in terms of tracking performance. The parameters of both controllers after being well-tuned are provided in Table 3.

Table 3. Parameters of the discrete-time fractional order integral sliding mode control (DFISMC) and conventional DSMC controller.

Parameters	FDISMC		DSMC	
	α	K_I	λ	K_{sw}
Values	0.8	0.01	0.1	1.5×10^{-3}

4.2. Experiment Result

To quantitatively evaluate the tracking performance, the maximum tracking error (MTE) and root mean square tracking error (RMSTE) are computed. The RMSTE is calculated as follows:

$$RMSTE = \sqrt{\frac{1}{N} \sum_{k=0}^N e_k^2}, \quad (22)$$

where N is the total number of data samples, and e_k is the tracking error under k^{th} sample.

Figure 4 depicts the experimental results when the actuator tracks the sine wave signals without load. The sinusoidal signal had an amplitude of 20° and frequency from 0.2 Hz to 1 Hz. In the second scenario, a knee gait pattern was given as a desired trajectory. The proposed controller was evaluated with two different gait cycle (GC) times: 2.5 s and 4 s. The experimental results of this scenario are shown in Figure 5. In both Figures 4 and 5, the upper sub-figure of each image includes the desired trajectory (black line), measured angle controlled by DFISM (dash-blue line), and measured angle controlled by conventional DSMC (dash-dot red line). The lower part of each figure shows the tracking errors of both proposed controller and DSMC controller. In comparison with the traditional DSMC, the DFISM was able to provide a better performance in both transient and steady states. As demonstrated in Figure 6, in all scenarios of the experiment, both MTE and RMSTE of the proposed control approach are smaller than the ones of the conventional DSMC control method. For example, when tracking the 1.0 Hz frequency sinusoidal signal, the RMSTEs of the DFISM and DSMC controllers are 1.63° and 1.43° , respectively. It means that DFISM is able to provide a better performance than the conventional DSMC controller. In particular, as seen in the error graphs in Figures 4 and 5, the finite amplitude oscillation of the tracking error in DFISM is much smaller than in DSMC. It can be concluded that the inherent “chattering” phenomenon of SMC control is reduced with DFISM. The numerical values of the experimental results in all scenarios are given in Table 4.

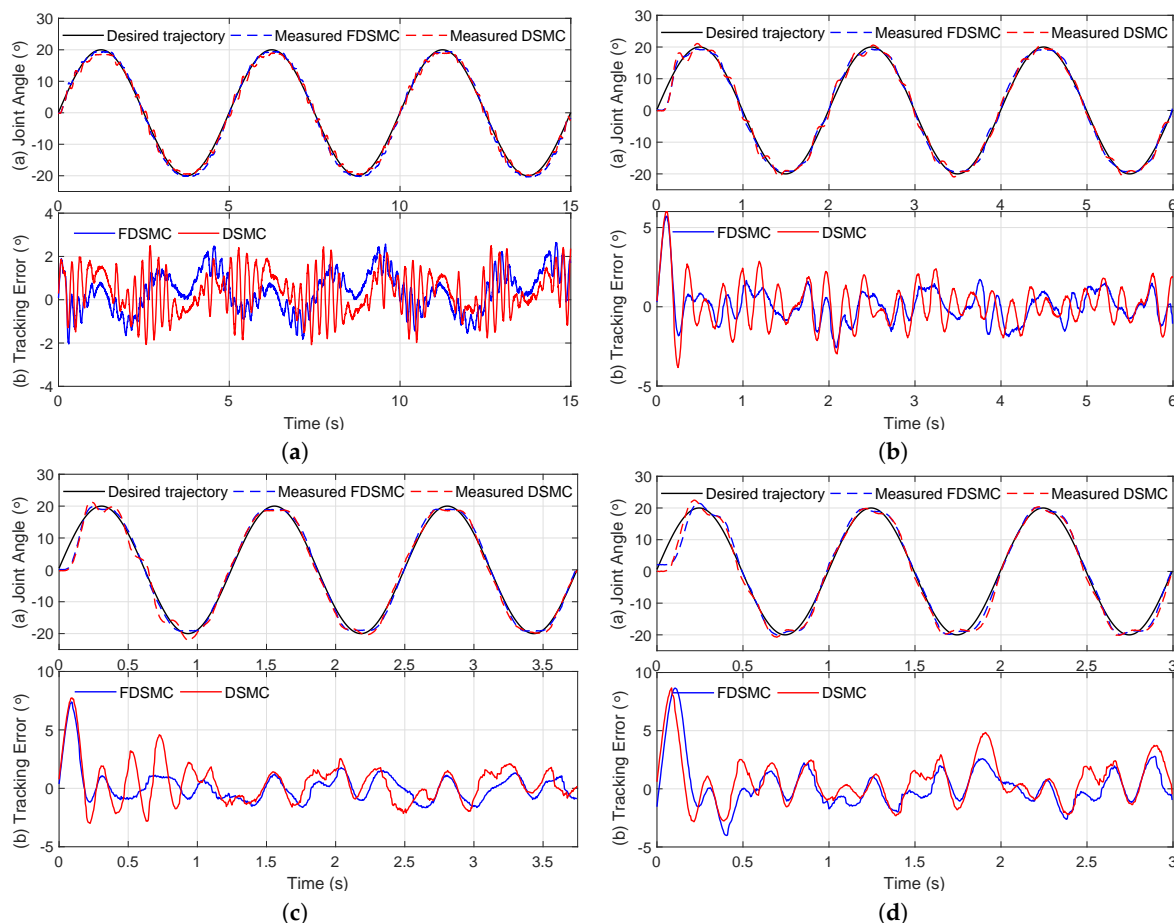


Figure 4. Experiment results without a load for tracking a sinusoidal trajectory: (a) 0.2 Hz, (b) 0.5 Hz, (c) 0.8 Hz, and (d) 1.0 Hz of signal frequency.

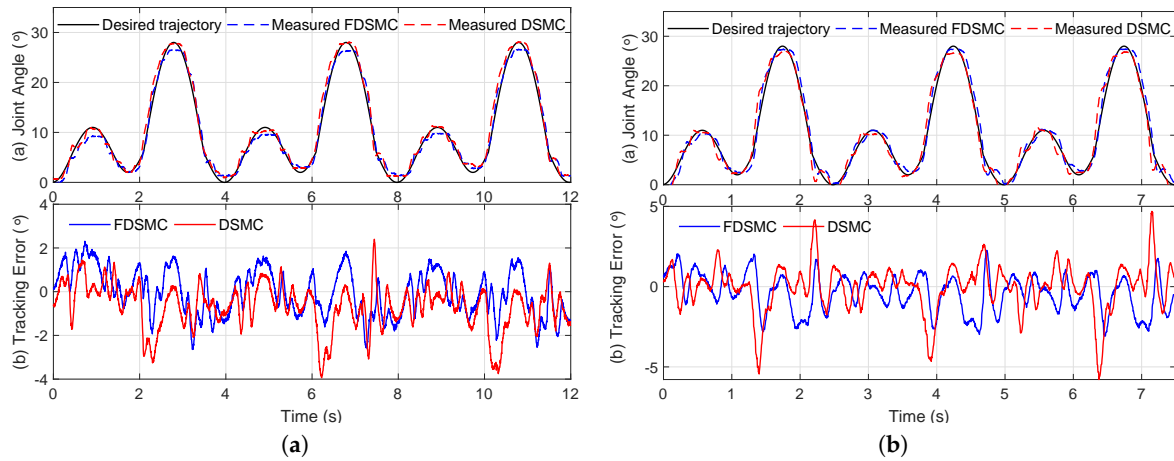


Figure 5. Experiment results of the proposed controller and conventional DSMC controller when tracking the human-gait pattern signal: (a) 4 s and (b) 2.5 s of gait cycle time. The experiment was carried out without a load.

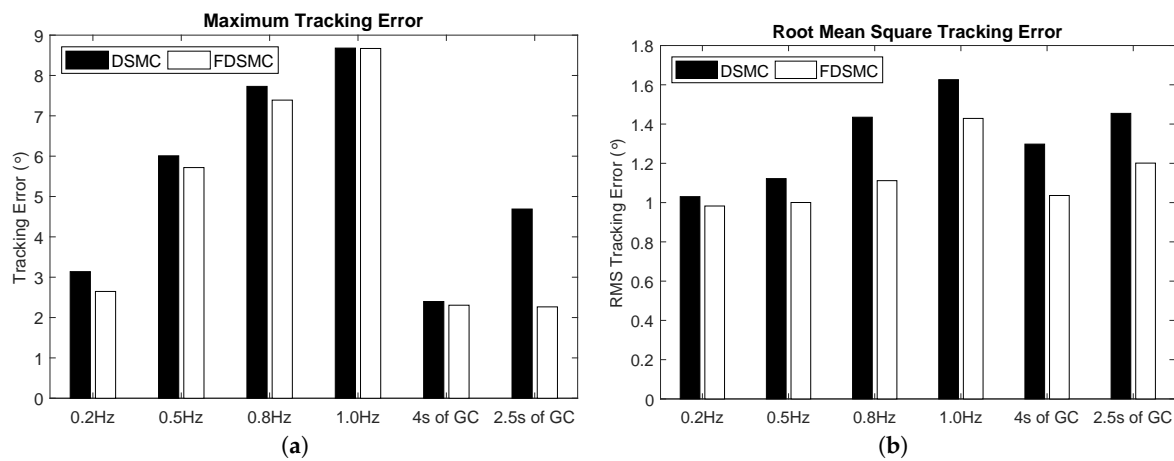


Figure 6. Maximum tracking error (MTE) and root mean square tracking error (RMSTE) of the proposed controller and conventional DSMC controller with 0.2 Hz, 0.5 Hz, 0.8 Hz, and 1.0 Hz of the desired signal frequency in case of no load.

Table 4. Maximum tracking error (MTE) and root mean square tracking error (RMSTE) of the proposed control method and conventional DSMC control method in case of no load.

Signal Frequency	MTE (°)		RMSTE (°)	
	DSMC	DFISMFC	DSMC	DFISMFC
0.2 Hz	3.14	2.65	1.03	0.98
0.5 Hz	6.01	5.71	1.12	1.00
0.8 Hz	7.73	7.39	1.43	1.11
1.0 Hz	8.68	8.67	1.63	1.43
4 s of GC	2.40	2.31	1.30	1.04
2.5 s of GC	4.69	2.26	1.45	1.20

Figures 7 and 8 show the control performances of the system when tracking the sinusoidal signals and human-gait pattern with a load of 2.5 kg, respectively. When the antagonistic actuator carries a load $m = 2.5$ kg, the difference between the DFISMFC and DSMC is not significant in terms of MTE. However, the RMSTE of the DFISMFC controller are smaller than the ones of the DSMC controller, as shown in Figure 9. For example, when tracking the 2.5 s human-gait trajectory, the RMSTEs of the DFISMFC and DSMC controllers are 1.22° and 1.68° , respectively. Furthermore, the same conclusion

about the “chattering” phenomenon is drawn out in this experiment scenario. All numerical values of MTE and RMSTE in this experimental scenario are also shown in Table 5.

From experimental results with multiple scenarios, we can conclude that the DFISM controller obtains a better tracking performance than the conventional DSMC controller which used the “sign” function of tracking errors. In addition, the implemented disturbance observer and fractional order integral term are able to deal with the finite-amplitude oscillation of sliding mode implementations. As a result, the “chattering” phenomenon is reduced.

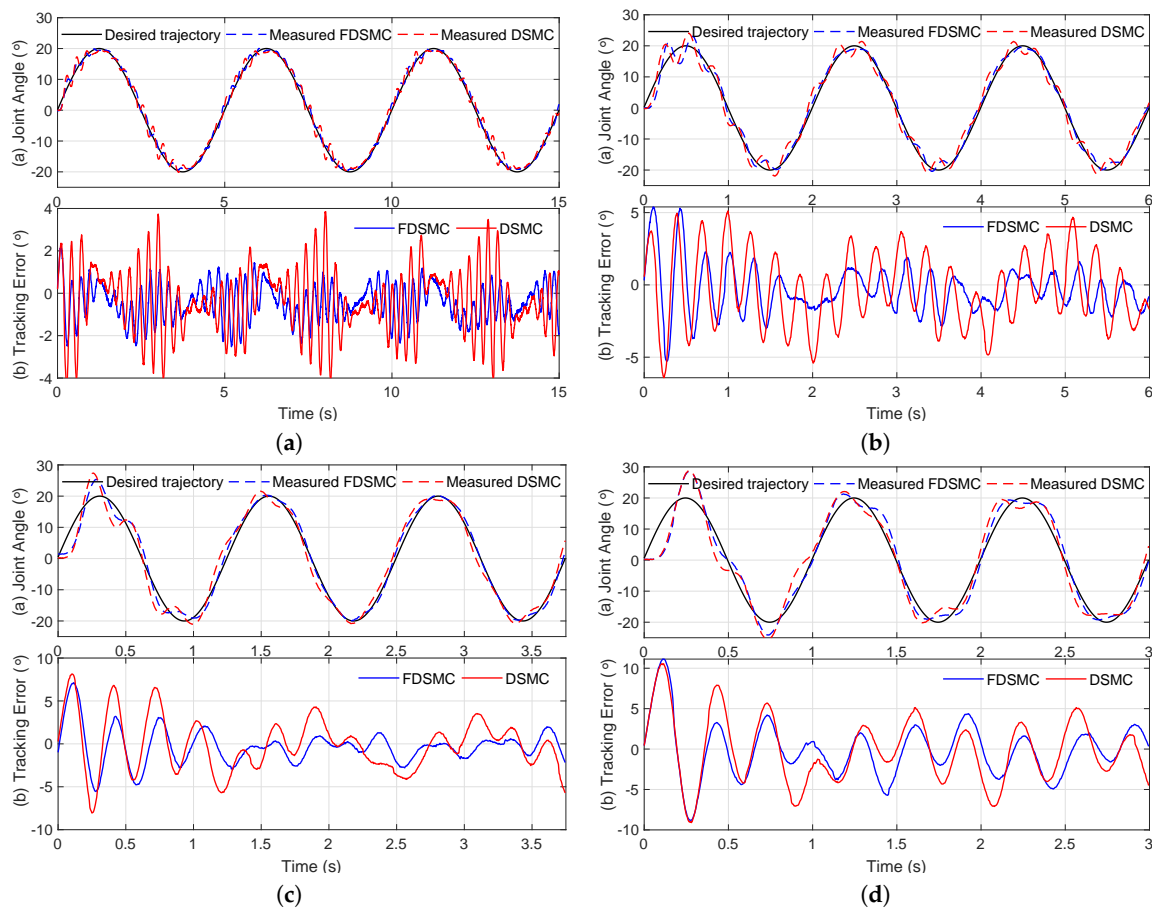


Figure 7. Experiment results with 2.5 kg of load for tracking a sinusoidal trajectory: (a) 0.2 Hz, (b) 0.5 Hz, (c) 0.8 Hz, and (d) 1.0 Hz of the desired signal frequency.

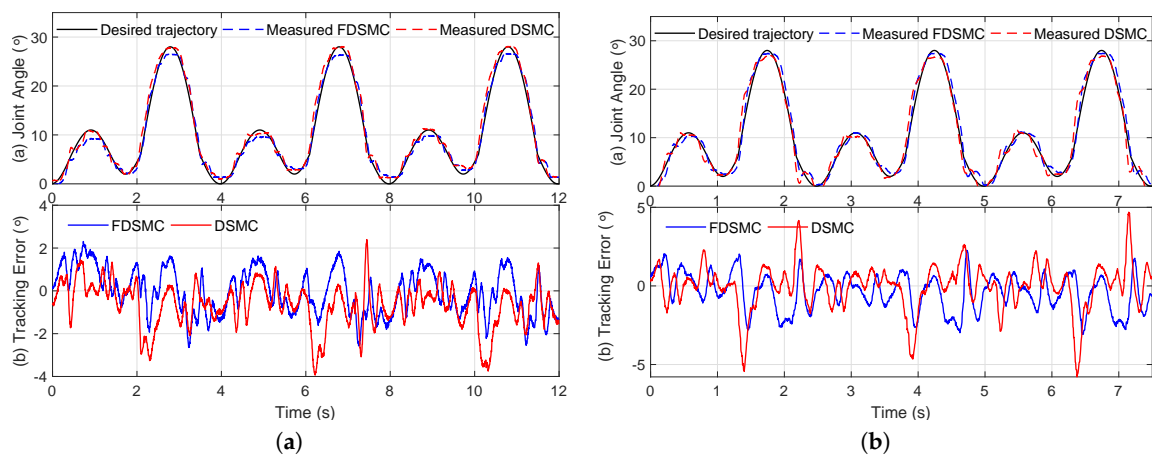


Figure 8. Experiment results for the proposed controller and conventional DSMC controller when tracking the human-gait pattern signal with a load $m = 2.5$ kg: (a) 4 s and (b) 2.5 s of gait cycle time.

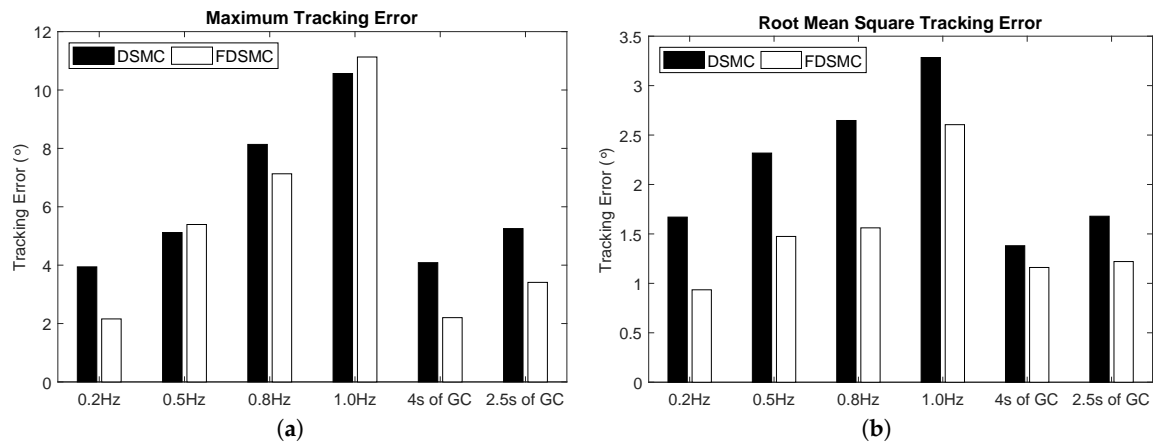


Figure 9. MTE and RMSTE of the proposed controller and conventional DSMC controller with 0.2 Hz, 0.5 Hz, 0.8 Hz, and 1.0 Hz of the desired signal frequency and load $m = 2.5$ kg.

Table 5. MTE and RMSTE of the proposed control method and conventional DSMC control method with load $m = 2.5$ kg.

Signal Frequency	MTE (°)		RMSTE (°)	
	DSMC	DFISMC	DSMC	DFISMC
0.2 Hz	3.94	2.16	1.67	0.93
0.5 Hz	5.11	5.39	2.31	1.47
0.8 Hz	8.13	7.13	2.64	1.56
1.0 Hz	10.56	11.13	3.28	2.61
4 s of GC	4.09	2.20	1.38	1.16
2.5 s of GC	5.23	3.41	1.68	1.22

5. Discussion and Conclusions

This paper proposed an advanced SMC control strategy for PAMs in antagonistic configuration. First, the discrete-time SOPDT is chosen to describe the dynamic behaviour of the antagonistic actuator. The chosen model demonstrated a good approximation of nonlinear characteristics of the actuator: the root mean square errors between estimated and measured values are less than 2.5° . Based on the built-in model, an DFISM C controller, which employed a fractional order integral of tracking error together with a disturbance observer, was proposed for the tracking purpose. The implemented approximation of FOI and DO was able to reduce the “chattering” phenomenon, which often occurs in SMC implementations. The reduction of the “chattering” phenomenon is very important for applications of the PAMs in rehabilitation robot field. Finally, multi-scenario experiments were carried out to compare the tracking performances between the DFISM C and the conventional DSMC.

In comparison with the three-elements model [5], hysteresis model [13–15], and mechanism-based model [22,23], the identification procedure of the proposed method is simplified. Besides, this procedure does not need to measure the load’s acceleration, which is very sensitive to noise. Experiments show that, in comparison with DSMC, the DFISM C was able to significantly enhance the tracking performance of 20° amplitude sinusoidal signals with frequency up to 1.0 Hz. In particular, when the actuator drove a load of $m = 2.5$ kg, the RMSTEs of DFISM C were about two times less than those of conventional DSMC in most of the desired trajectory frequencies. For example, with a frequency of 0.2 Hz, the RMSTEs are 0.93° and 1.67° for DFISM C and DSMC, respectively. The proposed controller achieves a performance comparable to the experimental results with similar configuration and desired trajectory in [23,24]. In [23], when tracking a 0.4 Hz frequency and 5° sinusoidal signal, the residual error amplitude is 0.5° equivalent to 10%. When tracking a 0.5 Hz frequency and 20° amplitude sinusoidal signal, the RMSTE of the DFISM C is 1.47° , equivalent to

7.35% of amplitude. This result was better than the one in [24], in which a sinusoidal signal with 40° amplitude and frequency 0.25 Hz is used as a desired trajectory. The experiments also show that the proposed controller can track a human-gait pattern with the MTE of less than 6°. This result is in accordance with the commercial gait training system LOKOMAT [30], in which the MTE is 15°. It is shown that the built-in model and proposed controller can be applied in robot gait training system. Furthermore, the proposed DFISMCMC is designed in discrete-time domain, so that it is convenient for implementing in any digital industrial controller, e.g., the NI instrument in this research.

In summary, this paper presents the control of an antagonistic actuator powered by PAMs. The dynamic behaviour of the antagonistic actuator is described by a discrete-time SOPDT model, which requires a simpler identification procedure. The DFISMCMC controller based on a DSO and the approximated FOI is used to improve the tracking performance. The implementation of DSO and FOI also helps the system reduce the “chattering” phenomenon. The experimental results illustrate the applicability of the proposed model and controller to a robotic gait training system with a human-gait pattern trackable ability. Future work will involve the impedance control of the antagonistic actuator to increase applicability of PAMs in the field of rehabilitation. The impedance of the actuator can be regulated by manipulating the nominal pressure P_0 of two PAMs. To integrate the impedance controller into the system, the relationship between the actuator compliance and nominal pressure P_0 would be considered and modelled in future work.

Author Contributions: Q.-T.D. conceived the methodology and designed the experiment; he also performed the experiment. Q.-T.D. and M.-L.N. analyzed data and wrote the paper. S.-i.Y. led the research efforts and preparation of this paper.

Conflicts of Interest: The authors declare no conflict of interest.

Abbreviations

The following abbreviations are used in this manuscript:

PAM	Pneumatic artificial muscle
PID	Proportional integral derivative
SOPDT	Second order plus dead time
SISO	Single input single output
SMC	Sliding mode control
DSMC	Discrete-time sliding mode control
DFISMCMC	Discrete-time fractional order integral sliding mode control
MTE	Maximum tracking error
RMSTE	Root mean square tracking error
ESO	Extended state observer
ADRC	Active disturbance rejection controller
DSO	Disturbance observe
SD	Standard deviation
FOI	Fractional order integral
GC	Gait cycle

Appendix A. Fractional Integral Approximation

Fractional-order calculus is a generalization of the integration and differentiation from integer to non-integer order. This appendix introduces only definitions which are widely used in the area of control systems. First, gamma function $\Gamma(z)$, which is the extension of the factorial for non-integer number z , is introduced as

$$\Gamma(z) = \int_0^{\infty} e^{-t} t^{z-1} dt \quad (\text{A1})$$

The most important property of the gamma function is

$$z\Gamma(z) = \Gamma(z + 1) \quad (\text{A2})$$

Then, the definition of integral of order $\alpha \in \mathbb{R}$ is presented. In continuous-time domain, the most often used one is the *Riemann-Liouville* definition:

$${}^{\alpha}\Xi e(t) = \frac{1}{\Gamma(\alpha)} \int_0^t (t - \tau)^{(\alpha-1)} e(\tau) d\tau \tag{A3}$$

At this time, the FOI is not supported in any programming language. For this reason, its numerical approximation is required to implement the FOI in any real-time control system. In a digital control system with sampling time T_s , interval $(0, t)$ can be approximated by $k = \frac{t}{T_s}$ sub-intervals. Therefore,

$${}^{\alpha}\Xi e(t) = \frac{1}{\Gamma(\alpha)} \sum_{j=1}^k \int_{jT_s}^{(j+1)T_s} (t - \tau)^{(\alpha-1)} e(\tau) d\tau \tag{A4}$$

Consider that T_s is small enough, so that e is constant in each sub-interval. Therefore,

$${}^{\alpha}\Xi e(t) \approx {}^{\alpha}\Xi_{e,k} = \frac{1}{\Gamma(\alpha)} \sum_{j=1}^k \int_{jT_s}^{(j+1)T_s} (t - \tau)^{(\alpha-1)} e(\tau) d\tau \tag{A5}$$

Following that,

$${}^{\alpha}\Xi_{e,k} = \sum_{j=1}^k [(k - j + 1)^{\alpha} - (k - j)^{\alpha}] \frac{T_s^{\alpha}}{\alpha\Gamma(\alpha)} e_{j+1} \tag{A6}$$

From (A2) and (A6), we have

$${}^{\alpha}\Xi_{e,k} = \sum_{j=1}^k \omega_j e_j \tag{A7}$$

with the weighting factor ω_j as follows:

$$\omega_j = [(k - j + 1)^{\alpha} - (k - j)^{\alpha}] \frac{T_s^{\alpha}}{\alpha\Gamma(\alpha)}. \tag{A8}$$

Because of the infinite data in (A7), the approximation of FIO cannot be directly implemented in any digital system. In this research, the recursive approximation of FIO in [31] is employed. Denote $\Xi_{e,k-1}$ as FIO of the tracking error in the last step, and it can be computed as

$${}^{\alpha}\Xi_{e,k-1} = \sum_{j=2}^k \omega_j e_{j-1} \tag{A9}$$

From (A7) and (A9), we have

$${}^{\alpha}\Xi_{e,k} = {}^{\alpha}\Xi_{e,k-1} + \sum_{j=2}^k \omega_j \tilde{e}_{j-1} + \omega_1 e_1 \tag{A10}$$

where $\tilde{e}_j = e_j - e_{j-1}$. We apply the short memory principle to (A10) and we can consider two cases:

(a). If $k < N$, where $N = \left\lceil \frac{L}{T_s} \right\rceil$ is the number of considered data samples, then

$${}^{\alpha}\Xi_{e,k} = {}^{\alpha}\Xi_{e,k-1} + \sum_{j=N-k+2}^N \Omega_j \tilde{e}_{N-k+j} + \Omega_{N-k+1} e_1 \tag{A11}$$

(b). If $k \geq N$,

$${}^\alpha \Xi_{e,k} = {}^\alpha \Xi_{e,k-1} + \sum_{j=2}^N \Omega_j \tilde{e}_{k-N+j} + \Omega_1 e_{k-N+1} \tag{A12}$$

where

$$\Omega_j = [(N - j + 1)^\alpha - (N - j)^\alpha] \frac{T_s^\alpha}{\Gamma(\alpha + 1)} \tag{A13}$$

The FIO is approximated by Equations (A11) and (A12), which can be easily implemented in any digital control system.

Appendix B. Proof of Assumption 1

Assumption 1 is based on the Taylor expansion and can be explained as follows. For a very small constant T_s , we have

$$p(t - T_s) = p(t) - \frac{dp(t)}{dt} T_s + \sum_{i=2}^{\infty} (-1)^i \frac{d^{(i)} p(t)}{dt^i} \frac{T_s^i}{i!} \tag{A14}$$

Then, it can be derived from (A14) that

$$\begin{aligned} p(t) - p(t - T_s) &= \frac{dp(t)}{dt} T_s - \sum_{i=2}^{\infty} (-1)^i \frac{d^{(i)} p(t)}{dt^i} \frac{T_s^i}{i!} \\ &\approx \frac{dp(t)}{dt} T_s + O(T_s^2) \end{aligned} \tag{A15}$$

Assume that signal $p(t)$ is smooth, and its differential is bounded. Then there exists a constant A such that

$$|p(t) - p(t - T_s)| \leq AT_s + O(T_s^2) \tag{A16}$$

which means

$$P(t) - p(t - T_s) = O(T_s) \tag{A17}$$

and (12) holds.

Now, ignore the small term $O(T_s^2)$ and differentiate both sides of (A15). This gives us

$$\frac{dp(t)}{dt} - \frac{dp(t - T_s)}{dt} \approx \frac{d^2 p(t)}{dt^2} T_s \tag{A18}$$

By using (A15) on the left side of (A18),

$$p(t) - 2p(t - T_s) + p(t - 2T_s) \approx \frac{d^2 p(t)}{dt^2} T_s^2 \tag{A19}$$

Again, assume that the second order differential of $p(t)$ is bounded by a constant B , then it leads to

$$|p(t) - 2p(t - T_s) + p(t - 2T_s)| \leq BT_s^2 \tag{A20}$$

which means that (15) holds.

References

1. Banala, S.K.; Kim, S.H.; Agrawal, S.K.; Scholz, J.P. Robot Assisted Gait Training with Active Leg Exoskeleton (ALEX). *IEEE Trans. Neural Syst. Rehabil. Eng.* **2009**, *17*, 2–8. [[CrossRef](#)]
2. Beyl, P.; Knaepen, K.; Duerinck, S.; Van Damme, M.; Vanderborght, B.; Meeusen, R.; Lefeber, D. Safe and Compliant Guidance by a Powered Knee Exoskeleton for Robot-Assisted Rehabilitation of Gait. *Adv. Robot.* **2011**, *25*, 513–535. [[CrossRef](#)]
3. Dao, Q.-T.; Yamamoto, S.-I. Assist-as-Needed Control of a Robotic Orthosis Actuated by Pneumatic Artificial Muscle for Gait Rehabilitation. *Appl. Sci.* **2018**, *8*, 499. [[CrossRef](#)]
4. Hussain, S.; Xie, S.Q.; Jamwal, P.K. Control of a robotic orthosis for gait rehabilitation. *Robot. Auton. Syst.* **2013**, *61*, 911–919. [[CrossRef](#)]
5. Reynolds, D.B.; Repperger, D.W.; Phillips, C.A.; Bandry, G. Dynamic characteristics of pneumatic muscle. *Ann. Biomed. Eng.* **2003**, *31*, 310–317. [[CrossRef](#)]
6. Xing, K.; Huang, J.; Wang, Y.; Wu, J.; Xu, Q.; He, J. Tracking control of pneumatic artificial muscle actuators based on sliding mode and non-linear disturbance observer. *IET Control Theory Appl.* **2010**, *4*, 2058–2070. [[CrossRef](#)]
7. Lilly, J.H.; Quesada, P.M. A two-input sliding-mode controller for a planar arm actuated by four pneumatic muscle groups. *IEEE Trans. Neural Syst. Rehabil. Eng.* **2004**, *12*, 349–359. [[CrossRef](#)]
8. Lilly, J.H.; Yang, L. Sliding mode tracking for pneumatic muscle actuators in opposing pair configuration. *IEEE Trans. Control Syst. Technol.* **2005**, *13*, 550–558. [[CrossRef](#)]
9. Choi, T.Y.; Lee, J.J. Control of Manipulator Using Pneumatic Muscles for Enhanced Safety. *IEEE Trans. Ind. Electron.* **2010**, *57*, 2815–2825. [[CrossRef](#)]
10. Choi, T.Y.; Choi, B.S.; Seo, K.H. Position and Compliance Control of a Pneumatic Muscle Actuated Manipulator for Enhanced Safety. *IEEE Trans. Control Syst. Technol.* **2011**, *19*, 832–842. [[CrossRef](#)]
11. Hussain, S.; Xie, S.Q.; Jamwal, P.K. Adaptive Impedance Control of a Robotic Orthosis for Gait Rehabilitation. *IEEE Trans. Cybern.* **2013**, *43*, 1025–1034. [[CrossRef](#)]
12. Merola, A.; Colacino, D.; Cosentino, C.; Amato, F. Model-based tracking control design, implementation of embedded digital controller and testing of a biomechanical device for robotic rehabilitation. *Mechatronics* **2018**, *52*, 70–77. [[CrossRef](#)]
13. Minh, T.V.; Tjahjowidodo, T.; Ramon, H.; Brussel, H.V. Cascade position control of a single pneumatic artificial muscle-mass system with hysteresis compensation. *Mechatronics* **2010**, *20*, 402–414. [[CrossRef](#)]
14. Xie, S.; Mei, J.; Liu, H.; Wang, Y. Hysteresis modeling and trajectory tracking control of the pneumatic muscle actuator using modified Prandtl–Ishlinskii model. *Mech. Mach. Theory* **2018**, *120*, 213–224. [[CrossRef](#)]
15. Kosaki, T.; Minesaki, A.; Sano, M. Adaptive Hysteresis Compensation with a Dynamic Hysteresis Model for Control of a Pneumatic Muscle Actuator. *J. Environ. Eng.* **2012**, *7*, 53–65. [[CrossRef](#)]
16. Vo-Minh, T.; Tjahjowidodo, T.; Ramon, H.; Brussel, H.V. A new approach to modeling hysteresis in a pneumatic artificial muscle using the Maxwell-slip model. *IEEE/ASME Trans. Mechatron.* **2011**, *16*, 177–186. [[CrossRef](#)]
17. Minh, T.V.; Kamers, B.; Ramon, H.; Brussel, H.V. Modeling and control of a pneumatic artificial muscle manipulator joint- part i: Modeling of a pneumatic artificial muscle manipulator joint with accounting for creep effect. *Mechatronics* **2012**, *22*, 923–933. [[CrossRef](#)]
18. Ba, D.X.; Ahn, K.K. Indirect sliding mode control based on gray-box identification method for pneumatic artificial muscle. *Mechatronics* **2015**, *32*, 1–11. [[CrossRef](#)]
19. Ba, D.X.; Dinh, T.Q.; Ahn, K.K. An integrated intelligent nonlinear control method for a pneumatic artificial muscle. *IEEE/ASME Trans. Mechatron.* **2016**, *21*, 1835–1845. [[CrossRef](#)]
20. Robinson, R.M.; Kothera, C.S.; Sanner, R.M.; Wereley, N.M. Nonlinear Control of Robotic Manipulators Driven by Pneumatic Artificial Muscles. *IEEE/ASME Trans. Mechatron.* **2016**, *21*, 55–68. [[CrossRef](#)]
21. Cveticanin, L.; Zukovic, M.; Biro, I.; Sarosi, J. Mathematical investigation of the stability condition and steady state position of a pneumatic artificial muscle—Mass system. *Mech. Mach. Theory* **2018**, *125*, 196–206. [[CrossRef](#)]
22. Yang, H.; Yu, Y.; Zhang, J. Angle tracking of a pneumatic muscle actuator mechanism under varying load conditions. *Control Eng. Pract.* **2017**, *61*, 1–10. [[CrossRef](#)]

23. Zhao, L.; Li, Q.; Liu, B.; Cheng, H. Trajectory Tracking Control of a One Degree of Freedom Manipulator Based on a Switched Sliding Mode Controller with a Novel Extended State Observer Framework. *IEEE Trans. Syst. Man Cybern. Syst.* **2019**, *49*, 1110–1118. [[CrossRef](#)]
24. Andrikopoulos, G.; Nikolakopoulos, G.; Manesis, S. Advanced Nonlinear PID-Based Antagonistic Control for Pneumatic Muscle Actuators. *IEEE Trans. Ind. Electron.* **2014**, *61*, 6926–6937. [[CrossRef](#)]
25. Yuan, Y.; Yu, Y.; Guo, L. Nonlinear Active Disturbance Rejection Control for the Pneumatic Muscle Actuators With Discrete-Time Measurements. *IEEE Trans. Ind. Electron.* **2019**, *66*, 2044–2053. [[CrossRef](#)]
26. Zhao, L.; Liu, X.; Wang, T. Trajectory tracking control for double-joint manipulator systems driven by pneumatic artificial muscles based on a nonlinear extended state observer. *Mech. Syst. Signal Process.* **2019**, *122*, 307–320. [[CrossRef](#)]
27. Zhao, L.; Cheng, H.; Xia, Y.; Liu, B. Angle Tracking Adaptive Backstepping Control for a Mechanism of Pneumatic Muscle Actuators via an AESO. *IEEE Trans. Ind. Electron.* **2019**, *66*, 4566–4576. [[CrossRef](#)]
28. Yuan, Y.; Yu, Y.; Wang, Z.; Guo, L. A Sampled-Data Approach to Nonlinear ESO-Based Active Disturbance Rejection Control for Pneumatic Muscle Actuator Systems with Actuator Saturations. *IEEE Trans. Ind. Electron.* **2019**, *66*, 4608–4617. [[CrossRef](#)]
29. Winter, D.A. *Biomechanics and Motor Control of Human Movement*, 3rd ed.; University of Waterloo Press: Waterloo, ON, Canada, 1990.
30. Riener, R.; Lunenburger, L.; Jezernik, S.; Anderschitz, M.; Colombo, G.; Dietz, V. Patient-cooperative strategies for robot-aided treadmill training: First experimental results. *IEEE Trans. Neural Syst. Rehabil. Eng.* **2005**, *13*, 380–394. [[CrossRef](#)]
31. Nguyen, M.L.; Chen, X. Discrete-Time Fractional Order Integral Sliding Mode Control for Piezoelectric Actuators with Improved Performance Based on Fuzzy Tuning. In Proceedings of the 2018 13th World Congress on Intelligent Control and Automation (WCICA), Changsha, China, 4–8 July 2018; pp. 554–559. [[CrossRef](#)]



© 2019 by the authors. Licensee MDPI, Basel, Switzerland. This article is an open access article distributed under the terms and conditions of the Creative Commons Attribution (CC BY) license (<http://creativecommons.org/licenses/by/4.0/>).